Materials Horizons

Accepted Manuscript

This article can be cited before page numbers have been issued, to do this please use: X. Yu, J. Joseph and A. Manthiram, *Mater. Horiz.*, 2016, DOI: 10.1039/C6MH00043F.

ROYAL SOCIETY OF CHEMISTRY

rsc.li/materials-horizons

View Article Online
DOI: 10.1039/C6MH00043F

Materials Horizons

COMMUNICATION

Suppression of the polysulfide-shuttle behavior in Li-S batteries through the development of a facile functional group on the polypropylene separator

Received 00th January 20xx,
Accepted 00th January 20xx

DOI: 10.1039/x0xx00000x

www.rsc.org/

Xingwen Yu, Jorphin Joseph, and Arumugam Manthiram*

Towards suppressing the polysulfide-shuttle behavior in lithium-sulfur (Li-S) batteries, a facile functional group has strategically been developed on commercial polypropylene (PP) battery separator through a sequence of hydroxylating, grafting, and hydrolyzing processes. The Li-S cells with the modified PP separator shows significantly enhanced cyclability.

Conceptual insights

Charge-discharge of lithium-sulfur (Li-S) batteries involves a class of intermediate products existing as various polysulfide species. The long-chain polysulfides (Li_2S_n, $4 \leq n \leq 8$) are generally soluble in the electrolyte and, therefore, have a tendency of shuttling between the anode and the cathode through the separator along with the liquid electrolyte. Such a polysulfide-shuttle behavior seriously deteriorates the cycling performances of the Li-S batteries, which has been considered as one of the most critical issues hampering the development of Li-S battery technology. This study presents a strategic approach to suppress the polysulfide-shuttle behavior by developing a facile functional group on the polypropylene (PP) backbone of the separator. With a sequence of hydroxylating, grafting, and hydrolyzing processes, the resulting carboxyl functional group offers a negatively charged environment which not only promotes Li^+-ion transport but also suppresses the negatively charged polysulfide ions from migrating from the cathode to the anode. As a result, the Li-S batteries with the modified PP separator show significantly enhanced cycling performances with low charge-discharge polarization.

Introduction

The emerging secondary battery system with room-temperature lithium-sulfur (Li-S) chemistry is gaining much attention as one of the most promising next-generation energy storage technologies for a broad range of applications.[1-3] However, this battery technology is currently facing a critical obstacle due to a so-called "polysulfide-shuttle" behavior during cell operation.[4-10] Actually, the shuttling behaviour of the soluble intermediate products is a common issue for a number of analogous battery systems such as lithium-selenium (Li-Se) [11, 12] and the room-temperature sodium-sulfur (RT Na-S)[13] batteries. For the Li-S batteries, although a lot of efforts have been made to address such a challenge since it has been recognized many year ago, there is still a lack of reliable approaches. For instance, attempts in the development of the advanced cathode matrices or structural configurations can alleviate the polysulfide diffusion to a certain extent, but these approaches are not able to absolutely encapsulate the polysulfides in the cathode.[14-23] Use of a Li^+-ion conductive solid electrolyte can effectively prevent the migration of the polysulfide species through. But these approaches usually bring new problems due to the relatively low room-temperature conductivity of the currently available solid electrolytes and the brittleness of the ceramic materials.[24-28]

Modification of the porous Celgard separator by adding a carbon-based coating or a polymer coating to suppress the polysulfide migration has previously been studied[29, 30] to alleviate the polysulfide shuttling. However, addition of the carbon or polymer coating to the separator could introduce additional weight and decrease the energy density. Herein we present an alternative strategy to suppress the polysulfide-shuttle in Li-S batteries by a modification of the traditional polypropylene (PP) separator to form a facile carboxyl functional group on the PP backbone. This new approach does not have an impact on the weight of the cell. With the modified separator, the Li-S batteries show significantly enhanced capacity retention ability in comparison to the cells prepared with the unmodified PP separator. Mechanistic studies have also been performed towards the understanding of the cation/anion transport behavior at the functionalized Celgard interface. Relevant mechanisms regarding the polysulfide retention by the functionalized Celgard separator is proposed.

Materials Science & Engineering Program and Texas Materials Institute, The University of Texas at Austin, Austin, TX78712, USA.
E-mail: manth@austin.utexas.edu

Electronic Supplementary Information (ESI) available: SEM images of a fresh Celgard membrane and a modified Celgard membrane; Schematic of a Li II Mod-Celgard II Li-PS cell; Voltage profiles of the Li ‖ Mod-Celgard ‖ Li-PS cells during the first two representative cycles at C/10 rate; . See DOI: 10.1039/x0xx00000x

View Article Online
DOI: 10.1039/C6MH00043F

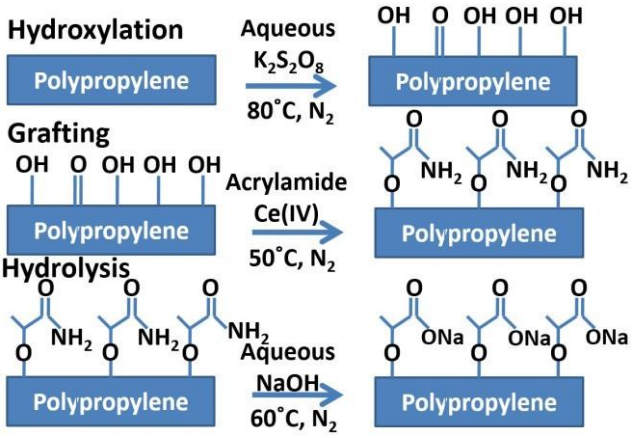

Fig. 1. Schematic of chemical modification of the polypropylene (PP) membrane through a sequence of hydroxylation, grafting, and hydrolysis processes.

Results and discussion

Modification of the Celgard membranes and characterization

Fig. 1 schematizes the modification processes of the polypropylene (PP, Celgard®2500) membrane according to a strategy reported previously,[31] majorly including the following three procedures: (1) hydroxylation of the membrane in alkaline solution, (2) grafting of acrylamide to the hydroxylated membrane, and (3) hydrolysis of the acrylamide-grafted membrane to form a carboxyl functional group on the membrane. The detailed modification processes are as provided in the experimental section. After the above modifications, the Celgard membrane does not change its morphology significantly, as reflected by the scanning electron microscope (SEM) images provided in Fig. S1.

Fig. 2a compares the Attenuated total reflection - Fourier transform infrared spectra (ART-FTIR) of the pristine PP separator with those of the modified separators at different modification stages. All the membrane samples show the characteristic bands of the PP separator: C-H stretching vibrations (2800 - 3000 cm^{-1}) and CH_2 bending vibrations (1450 - 1460 cm^{-1}). The broad O-H stretching peak (3400 - 3200 cm^{-1}) and the band due to C-O stretching (1100 cm^{-1})[32] observed for the hydroxyl functionalized Celgard membranes (Red linered in Fig. 2a) indicate the effective introduction of hydroxyl groups in to the Celgard membrane matrix. The hydroxylated membrane samples were retained in wet conditions and subjected to grafting reaction. The acrylamide grafting onto hydroxylated Celgard® 2500 was confirmed by the FTIR analysis of the film samples after washing and drying. The introduction of -CO-NH_2 group is evidenced by the appearance of N-H stretching peaks (doublet, 3200 and 3360 cm^{-1}), N-H bending peak (1664 cm^{-1}) and the C=O stretching peak of the amide (1630 cm^{-1}), as illustrated with the blue line in Fig. 2a. The green line in Fig. 2a displays the FTIR spectrum of the acrylamide grafted Celgard membrane after the hydrolysis with 1.0 M NaOH solution at 60° C for a period of 15 min followed by drying. The shift of the

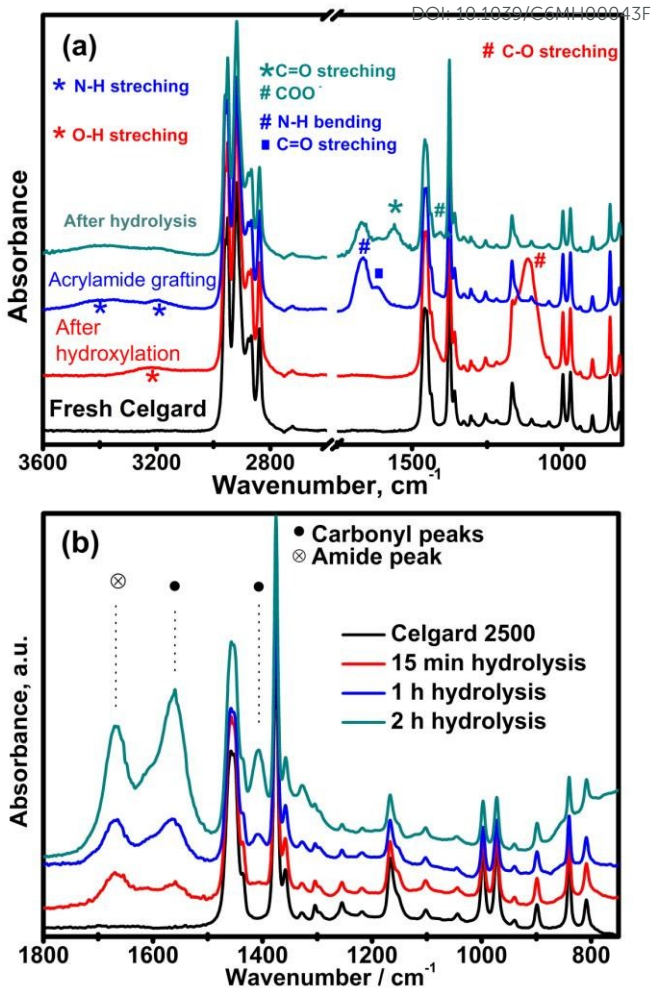

Fig. 2. (a) Attenuated total reflection - Fourier transform infrared (ART-FTIR) spectra of the fresh polypropylene (PP) membrane (black), after hydroxylation (red), after grafting (blue), and after the hydrolysis (green) processes, as schematized in Fig. 1. (b) ART-FTIR spectra of the acrylamide-grafted Celgard membranes that had been hydrolyzed for 15 min, 1 h, and 2 h.

carbonyl stretching peak from 1630 cm^{-1} to 1560 cm^{-1} and the appearance of a new peak at 1410 cm^{-1} indicate the conversion of grafted amide groups to sodium carboxylate groups.[32] The intensities of the carbonyl peaks of the carboxylate ion increases as the time of hydrolysis is enhanced from 15 min to 2 h (Fig. 2b), but the presence of amide peaks observed in the spectra of the films even after 2 h hydrolysis suggests that the hydrolysis achieved in these grafted membranes is not complete. However, from our experience, the 2-hour hydrolysis applied here had adversely influenced the mechanical integrity of the membranes.

Electrochemical performance of the Li-S cells with the modified Celgard membrane

The Li-S cells in this study were fabricated with a Li-metal anode, a dissolved Li-polysulfide (Li-PS) cathode, a liquid electrolyte comprising 1.0 M $LiCF_3SO_3$ and 0.1 M $LiNO_3$ dissolved in DME/DOL solvents (mixture of dimethoxy ethane

View Article Online
DOI: 10.1039/C6MH00043E

and 1, 3-dioxolane, with the volume ratio of 1 : 1), and the modified Celgard separator, as schematized in Fig. S2. The acrylamide-grafted Celgard membranes which had been hydrolyzed for 15 min and for 1 hour were used for the cell performance test, since the membrane subjected to a 2-hour hydrolysis showed poor mechanical properties. The resulting coin cells were, respectively, termed as Li II Mod(15 min)-Celgard II Li-PS cell and Li II Mod(1 h)-Celgard II Li-PS cell). For a comparison, the Li-S cells were also prepared with the unmodified Celgard membrane (termed as Li II Celgard II Li-PS cell). The Li-polysulfide cathode was prepared by dispersing the liquid Li-polysulfide catholyte into the carbon nanofiber (CNF) paper electrode as we previously presented.[33, 34] With the Li-polysulfide cathode, the cells can either be first charged or be first discharged (as illustrated in Fig. S3). Upon either an initial charge or an initial discharge, the following charge-discharge profiles showed the characteristics of the regular Li-S cells including two discharge plateaus and two charge plateaus (Fig. S3).

Fig. 3a, b, and c show the charge-discharge curves, respectively, of the Li II Celgard II Li-PS cell, Li II Mod(15 min)-Celgard II Li-PS cell, and Li II Mod(1 h)-Celgard II Li-PS cell at different C rates (the profiles at the 3rd cycle of each C-rate are shown here as representatives). Interestingly, the cells with the modified Celgard membranes (either 15 min or 1 h hydrolysis) show a less polarization behaviour than the Li II Celgard II Li-PS cell prepared with the unmodified Celgard separator. Table 1 summarizes the charge voltages, discharge voltages, and voltage gaps between the discharge and the charge profiles (derived from Fig. 3a, b, and c) of the three cells operated at different C rates. In each case, the charge or the discharge voltages were collected from the data shown in Fig. 3a, b, and c at the capacity value of 600 mAh g^{-1}. As seen in Table 1, the voltage gaps of the two cells with the modified Celgard membranes are lower than those of the Li II Celgard II Li-PS cell at each C rate. Also, the voltage gap increases with the increment of cycling rate for both the Li II Mod-Celgard II Li-PS cell and the Li II Celgard II Li-PS cell, but the cell with the unmodified Celgard membrane increases much more significantly. The cell with the Celgard membrane which had been subjected to a 1-hour hydrolysis shows the least polarization among the three cells. But the differences between the two cells with the modified Celgard membranes are not very significant.

Fig. 3d compares the cyclic voltammograms of the two Li II Mod-Celgard II Li-PS cells and the Li II Celgard II Li-PS cell (the CV profiles of the 3rd cycle of each cell are shown here as representatives). Modification of the Celgard shifts the discharge waves to a positive direction and the charge waves to a negative direction. The potential shifts in Fig. 3b are consistent with the polarization behaviour variations among the three cells shown in Fig. 3a-c. Fig. 3e displays the electrochemical impedance spectra (EIS, Nyquist plots) of the Li II Mod-Celgard II Li-PS cells and the Li II Celgard II Li-PS cell. It is speculated that the superior polarization behavior of the cell with the modified Celgard membranes was from the low internal impedance as

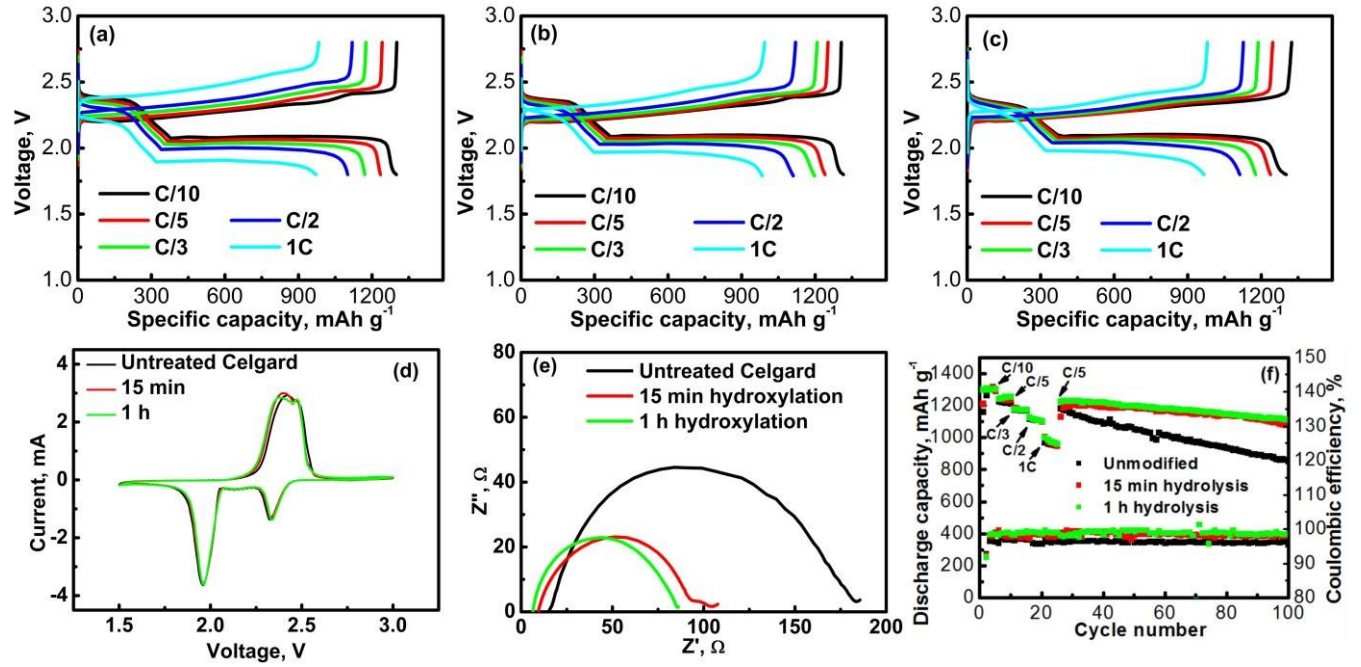

Fig. 3. Charge-discharge curves of the (a) Li II Celgard II Li-PS cell, (b) Li II Mod(15 min)-Celgard II Li-PS cell, and (c) Li II Mod(1 h)-Celgard II Li-PS cell at different C rates (the profiles at the 3rd cycle of each C rate are shown here as representatives). (d) Cyclic voltammetry (CV) profiles of the Li II Celgard II Li-PS cell, Li II Mod(15 min)-Celgard II Li-PS cell, and Li II Mod(1 h)-Celgard II Li-PS cell at a scan rate of 0.1 mV s^{-1} (the 3rd cycle of each cell is shown here as representatives). (e) Electrochemical impedance spectra (EIS) of the Li II Celgard II Li-PS cell, Li II Mod(15 min)-Celgard II Li-PS cell, and Li II Mod(1 h)-Celgard II Li-PS cell. (f) Discharge capacities and Coulombic efficiencies as a function of cycle number of the Li II Celgard II Li-PS cell, Li II Mod(15 min)-Celgard II Li-PS cell, and Li II Mod(1 h)-Celgard II Li-PS cell.

View Article Online
DOI: 10.1039/C6MH00011F

Table 1. The charge and the discharge voltages as well as the voltage gap between the charge and discharge of the Li II Celgard II Li-PS cell, Li II Mod(15 min)-Celgard II Li-PS cell, and Li II Mod(1 h)-Celgard II Li-PS cell at the charge/discharge capacity of 600 mAh g^{-1}. The data were derived from the charge/discharge curves in Fig. 3a, b, and c.

	Li II Celgard II Li-PS cell					Li II Mod-Celgard (15 min) II Li-PS cell					Li II Mod-Celgard (1 h) II Li-PS cell				
	C/10	C/5	C/3	C/2	1C	C/10	C/5	C/3	C/2	1C	C/10	C/5	C/3	C/2	1C
Charge voltage, V	2.27	2.29	2.33	2.37	2.48	2.26	2.27	2.28	2.33	2.40	2.26	2.27	2.28	2.30	2.38
Discharge voltage, V	2.08	2.06	2.03	2.00	1.90	2.09	2.07	2.06	2.04	1.96	2.10	2.08	2.07	2.05	1.98
Voltage gap, V	0.19	0.23	0.30	0.37	0.58	0.17	0.20	0.22	0.29	0.44	0.16	0.19	0.21	0.25	0.40

reflected from Fig. 3e. The modification of the Celgard membrane effectively decreased both the bulk impedance and the charge-transfer resistance of the Li–S cell according to the related EIS studies for the Li-S batteries.[35, 36]

Fig. 3f presents the long-term cycling performances of the two Li II Mod-Celgard II Li-PS cells and the Li II Celgard II Li-PS cell. It can be seen that the use of the modified Celgard membranes provides a significant advantage over the unmodified separator in terms of capacity retention during cycling. The three cells show similar initial discharge capacities at different C rates. However, the capacity degradation of the cell with the unmodified Celgard membrane is much faster. The capacity retention ability of the cells during the 100-cycle time frame is summarized in Table 2. The capacity fade-rate of the Li ‖ Celgard ‖ Li-PS cell is ~ 3 times of the two Li ‖ Mod-Celgard ‖ Li-PS cells. Also noticeably, the Coulombic efficiency of the Li ‖ Celgard ‖ Li-PS cell was is lower than those of the two Li ‖ Mod-Celgard ‖ Li-PS cells throughout the 100 cycles.

Post-mortem analyses of the cycled Celgard membranes

In order to understand the capacity retention effect from the modified Celgard, the separators taken out of the cycled cells (both the Li ‖ Mod(15 min)-Celgard ‖ Li-PS cell and the Li ‖ Celgard ‖ Li-PS cell) were analyzed with SEM/EDS. Fig. 4a-d presents the EDS elemental mappings of the cycled Celgard separator (unmodified). The element carbon was also mapped as a reference. There is a slight difference between the sulfur signals on the cycled Celgard that faces the anode (Fig. 4b) and that faces the cathode (Fig. 4d). However, as seen in Fig. 4e-h, for the modified Celgard, the sulfur signal is much higher at the cathode side (Fig. 4e) than that at the anode side (Fig. 4h). The above results clearly indicate that the modification of the Celgard membrane significantly improves its ability for suppressing the polysulfide-shuttle behavior during cycling.

Table 2. Initial capacity, 100th cycle capacity, capacity retention, and capacity fade-rate of the Li II Celgard II Li-PS cell, Li II Mod(15 min)-Celgard II Li-PS cell, and Li II Mod(1 h)-Celgard II Li-PS cell

	Initial capacity, mAh g^{-1}	100th cycle capacity, mAh g^{-1}	Capacity retention, %	Capacity fade rate, %
Li ‖ Celgard ‖ Li-PS	1220	850	69.7	0.30
Li ‖ Mod(15 min)-Celgard ‖ Li-PS	1240	1080	87.1	0.13
Li ‖ Mod(1 h)-Celgard ‖ Li-PS	1250	1115	89.2	0.11

Fig. 4i compares the FTIR-ATR spectra of the uncycled and cycled (after 100 cycles) mod-Celgard membrane (15 min hydrolysis). The spectrum of the cycled membrane (obtained after washing and drying) displayed all spectral features of the uncycled membrane, which indicates that the functional groups had been maintained at the surface of the Celgard membrane during cycling of the cell. The additional bands displayed on the spectrum of the cycled membrane are due to the bound Li salt ($LiCF_3SO_3$).

Mechanistic analyses

Form the results presented above, modification of the Celgard membrane brought two significant advantages towards improving the cycling performances of the Li-S batteries. From the reduced polarization behavior shown in Fig. 3a-c (also in Table 1), the desired voltage shifts shown in Fig. 3d and the improved impedance reduction shown in Fig. 3e, the carbonyl functional group developed on the Celgard membrane enhances the ionic interface between the membrane and the electrode, which promotes the electrochemical reactions. It has been generally recognized that the hydroxyl- and/or the

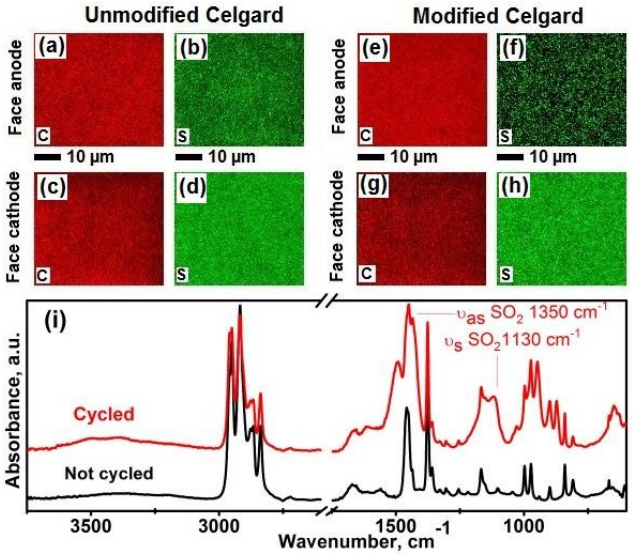

Fig. 4. (a-h) Energy dispersive spectroscopy (EDS) analyses of the cycled (after 100 cycles) Celgard membranes. The EDS mappings were collected on both sides of the membrane that faces the anode and that faces the cathode). (a-d) Elemental mappings (carbon and sulfur) of the cycled Celgard separator taken out of the Li II Celgard II Li-PS cell. (e-h) Elemental mappings (carbon and sulfur) of the cycled separator taken out the Li II Mod (15 min)-Celgard II Li-PS cell. (i) ART-FTIR spectra of the uncycled mod(15 min)-Celgard and the cycled (after 100 cycles) mod(15 min)-Celgard membranes.

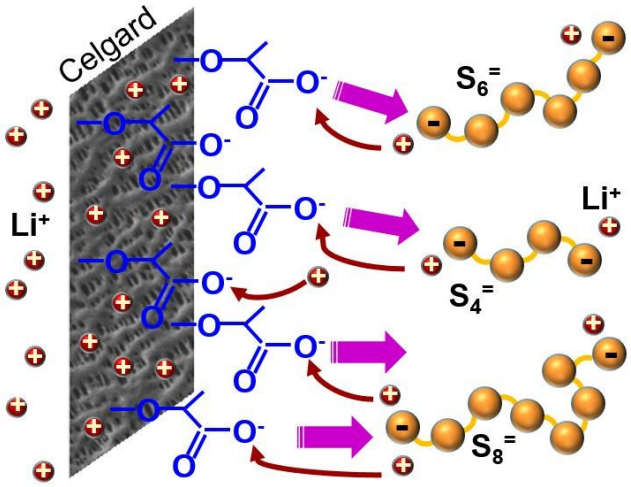

Fig. 5. Schematic of the ionic-selectivity of the modified Celgard membrane and the ionic interactions at the membrane-cathode interface.

carboxyl-functional groups are able to improve the hydrophilic properties of the PP separator.[31] Therefore, the modification of the Celgard in this study is deemed to engender a facile separator surface for the assessment of the solvents of the liquid electrolyte (DEM/DOL). On the other hand, the carboxyl functional group is expected to provide a facile negatively charged environment to promote the Li^+-ion transport (will be further discussed later).

During charge-discharge of a Li-S battery, the cathode side with the dissolved lithium polysulfides in organic solvents is a very complicated situation. The intermediate charge/discharge products exist as various forms of polysulfide species as generally considered as the soluble Li_2S_8, Li_2S_6, and Li_2S_4, and the insoluble Li_2S_2 *etc*.[37] In the real case for the Li-PS/solvent system, there also exist a variety of ionization and dissociation equilibria of the polysulfide species, as representatively illustrated with equations 1 and 2.[38-40] In either the non-dissociation or the dissociation case, due to the ionization of the Li-PS (eq. 1), the delithiated polysulfide ions (S_n^{2-}) or the free radicals ($S_{n/2}^{\cdot -}$) dissociated from the polysulfide ions (eq. 2) exist as the negatively charged species.

$$Li_2S_n \longrightarrow 2Li^+ + S_n^{2-} \quad (1)$$
$$S_n^{2-} \longrightarrow 2\, S_{n/2}^{\cdot -} \quad (2)$$

With the unmodified Celgard separator, the polysulfide ions and the free radicals are supposed to freely transfer through the neutral environment of the pores of the Celgard separator along with the Li-salts (*e. g.*, $LiCF_3SO_3$ and $LiNO_3$) and the solvent. However, upon modification, the carboxyl functional group formed on the PP backbone of the Celgard membrane provides a negatively charged environment at the pores of the Celgard membrane. Due to the "charge repulsion" effect, the resulting negatively charged environment can promote the transportation of the Li^+ ions with the positive charge but hinders the migration of the negatively charged polysulfide ions or the free radicals (dissociated from the polysulfide species). Therefore, the modified Celgard membrane plays a role likely as a cation-exchange membrane, as illustrated in Fig. 5.

Conclusions

With a sequence of hydroxylating, grafting, and hydrolyzing processes, a facile functional group gas strategically been developed on the polypropylene (PP) battery separator towards suppressing the polysulfide-shuttle behavior in the lithium-sulfur (Li-S) batteries. The Li-S cells with the modified PP separator show significantly enhanced cycling performances in comparison to the cells with the unmodified PP separators. Mechanistic studies reveal that the suppression of polysulfide migration through the modified separator is due to an electronic effects from the functional group at the separator/cathode interface.

Experimental

Materials and chemicals

The Celgard®2500 was obtained from Celgard LLC. Ammonium Cerium(IV) nitrate ($Ce(NH_4)_2(NO_3)_6$), potassium persulfate ($K_2S_2O_8$), and acrylamide ($CH_2CHCONH_2$) for modification of the Celgard membrane were purchased from Sigma Aldrich and used as received. Dimethoxy ethane (DME, 99+%), 1, 3-dioxolane (DOL, 99.5%), lithium trifluoromethanesulfonate ($LiCF_3SO_3$, 98%), lithium nitrate ($LiNO_3$, 99+%), sublimed sulfur powder (99.5 %), and lithium sulfide (Li_2S, 99.9 %) for preparation of the electrolyte and the polysulfide catholyte were purchased from Acros Organics and used as received. Carbon nanofiber (CNF) powder for preparation of the cathode matrix was obtained from Pyrograf Products Inc.

Modification of Celgard® 2500 films

A strategy reported previously by Garg *et al*[31] was adopted for the modification and grafting reaction on the Celgard membranes. Before the hydroxylation reaction, pieces of microporous polypropylene (PP) membranes were soaked in methanol and water for sufficiently wetting the surface and the pores of the films uniformly. The hydroxylation of the membranes were carried out by immersing these wet films in 10% $K_2S_2O_8$ solution with argon purging for a period of 2 h at 80˚C. The hydroxylated membranes were washed and dried at 60˚C for 24 h before chemical structure evaluation.

Hydroxylated membranes were subjected to grafting reaction at 50˚C under a stream of argon with a 2 mmol $Ce(NH_4)_2(NO_3)_6$ solution in 0.04 M nitric acid. The reaction was carried out for 1 h in presence of 3% (w/v) acrylamide in the medium. The grafted membranes were thoroughly washed with hot water and then in an ultrasonic bath to remove unreacted/non-bonded acrylamide. The acrylamide-grafted polypropylene membranes were hydrolysed by heating in 1.0 M sodium hydroxide solution at 60˚C under argon purge. Three different hydrolysis times (15 min, 1 h and 2 h) were applied to improve the amide to carboxylate conversion efficiency. These

modified membranes were then dried in vacuum at 60˚C for 24 h before chemical/electrochemical characterization.

Cell assembly and electrochemical experiments

Preparation of the cathode matrix (CNF paper electrodes) with the carbon nanofiber powder and the synthesis of Li_2S_6 polysulfide catholyte were as presented in our previous publications.[33, 34] The Li || Mod-Celgard (or unmodified Celgard) || Li-PS cells were prepared and tested with a coin cell configuration (CR 2032). The polysulfide cathodes were prepared by injectibg the synthesized lithium polysulfide catholyte into the CNF matrix with a net sulfur loading of 2.0 mg cm^{-2}. The mass ratio of the sulfur to the CNF matrix was 1 : 1. The cell assembly was performed in an Ar-filled glove box with the procedures as described in our previous publications.[33-35]

The cycling performances of the coin cells were tested on an Arbin® battery test station by galvanostatically charging and discharging the cells at different C rates. The charge-discharge capacities of the cells were calculated on the basis of the net sulfur materials in the cathodes. Cyclic voltammetry experiments were conducted on a VoltaLab PGZ402 potentiostat with a scan rate of 0.1 mV s^{-1}. Impedance of the coin cells was measured with a Solartron 1287 potentialstat.

Characterization

Scanning electron microscope (SEM) and energy dispersive spectroscometer (EDS) experiments were performed with a FEI Quanta 600 instrumentation. Fourier Transform Infrared Spectra (FTIR) of the pristine and modified membranes were recorded in Attenuated Total Reflectance (ATR) mode on a Thermo Scientific Nicolet iS5 instrument. 64 scans were added for each spectrum at a resolution of 4 cm^{-1}.

Acknowledgements

This work was supported by the Welch Foundation grant F-1254. One of the authors (J.J.) acknowledges the support from Sacred Heart College, Thevara-Kochi, India and financial support from Raman Postdoctoral fellowship, University Grants Commission (UGC), India.

Notes and references

1. A. Manthiram, S. H. Chung and C. X. Zu, *Adv Mater*, 2015, **27**, 1980-2006.
2. A. Manthiram, Y. Z. Fu, S. H. Chung, C. X. Zu and Y. S. Su, *Chem Rev*, 2014, **114**, 11751-11787.
3. Y. X. Yin, S. Xin, Y. G. Guo and L. J. Wan, *Angew Chem Int Edit*, 2013, **52**, 13186-13200.
4. A. Manthiram, Y. Z. Fu and Y. S. Su, *Accounts Chem Res*, 2013, **46**, 1125-1134.
5. D. Bresser, S. Passerini and B. Scrosati, *Chem Commun*, 2013, **49**, 10545-10562.
6. L. Chen and L. L. Shaw, *J Power Sources*, 2014, **267**, 770-783.
7. S. Evers and L. F. Nazar, *Accounts Chem Res*, 2013, **46**, 1135-1143.
8. L. Ma, K. E. Hendrickson, S. Y. Wei and L. A. Archer, *Nano Today*, 2015, **10**, 315-338. View Article Online DOI: 10.1039/C6MH00043F
9. M. K. Song, E. J. Cairns and Y. G. Zhang, *Nanoscale*, 2013, **5**, 2186-2204.
10. S. Zhang, K. Ueno, K. Dokko and M. Watanabe, *Adv Energy Mater*, 2015, **5**.
11. Y. X. Liu, L. Si, X. S. Zhou, X. Liu, Y. Xu, J. C. Bao and Z. H. Dai, *J Mater Chem A*, 2014, **2**, 17735-17739.
12. Y. X. Liu, L. Si, Y. C. Du, X. S. Zhou, Z. H. Dai and J. C. Bao, *J Phys Chem C*, 2015, **119**, 27316-27321.
13. X. W. Yu and A. Manthiram, *Adv Energy Mater*, 2015, **5**,1500305
14. C. J. Hart, M. Cuisinier, X. Liang, D. Kundu, A. Garsuch and L. F. Nazar, *Chem Commun*, 2015, **51**, 2308-2311.
15. J. X. Song, M. L. Gordin, T. Xu, S. R. Chen, Z. X. Yu, H. Sohn, J. Lu, Y. Ren, Y. H. Duan and D. H. Wang, *Angew Chem Int Edit*, 2015, **54**, 4325-4329.
16. T. Xu, J. X. Song, M. L. Gordin, H. Sohn, Z. X. Yu, S. R. Chen and D. H. Wang, *Acs Appl Mater Inter*, 2013, **5**, 11355-11362.
17. C. F. Zhang, H. B. Wu, C. Z. Yuan, Z. P. Guo and X. W. Lou, *Angew Chem Int Edit*, 2012, **51**, 9592-9595.
18. Y. Yang, G. H. Yu, J. J. Cha, H. Wu, M. Vosgueritchian, Y. Yao, Z. A. Bao and Y. Cui, *Acs Nano*, 2011, **5**, 9187-9193.
19. G. Q. Ma, Z. Y. Wen, J. Jin, Y. Lu, K. Rui, X. W. Wu, M. F. Wu and J. C. Zhang, *J Power Sources*, 2014, **254**, 353-359.
20. L. Wang, Z. H. Dong, D. Wang, F. X. Zhang and J. Jin, *Nano Lett*, 2013, **13**, 6244-6250.
21. Y. Z. Fu, Y. S. Su and A. Manthiram, *Acs Appl Mater Inter*, 2012, **4**, 6046-6052.
22. Y. Z. Fu and A. Manthiram, *Chem Mater*, 2012, **24**, 3081-3087.
23. Y. Z. Fu and A. Manthiram, *J Phys Chem C*, 2012, **116**, 8910-8915.
24. X. W. Yu, Z. H. Bi, F. Zhao and A. Manthiram, *Acs Appl Mater Inter*, 2015, **7**, 16625-16631.
25. L. Wang, Y. G. Wang and Y. Y. Xia, *Energ Environ Sci*, 2015, **8**, 1551-1558.
26. Q. S. Wang, J. Jin, X. W. Wu, G. Q. Ma, J. H. Yang and Z. Y. Wen, *Phys Chem Chem Phys*, 2014, **16**, 21225-21229.
27. A. Hayashi, T. Ohtomo, F. Mizuno, K. Tadanaga and M. Tatsumisago, *Electrochem Commun*, 2003, **5**, 701-705.
28. T. Kobayashi, Y. Imade, D. Shishihara, K. Homma, M. Nagao, R. Watanabe, T. Yokoi, A. Yamada, R. Kanno and T. Tatsumi, *J Power Sources*, 2008, **182**, 621-625.
29. S. H. Chung and A. Manthiram, *Adv Funct Mater*, 2014, **24**, 5299-5306.
30. J. Q. Huang, Q. Zhang, H. J. Peng, X. Y. Liu, W. Z. Qian and F. Wei, *Energ Environ Sci*, 2014, **7**, 347-353.
31. D. H. Garg, W. Lenk, S. Berwald, K. Lunkwitz, F. Simon and K. J. Eichhorn, *J Appl Polym Sci*, 1996, **60**, 2087-2104.
32. J. Coates, in *Encyclopedia of Analytical Chemistry*, ed. R. A. Meyers, John Wiley & Sons Ltd, 2006, pp. 10815-10837.
33. X. W. Yu and A. Manthiram, *Phys Chem Chem Phys*, 2015, **17**, 2127-2136.
34. Y. Z. Fu, Y. S. Su and A. Manthiram, *Angew Chem Int Edit*, 2013, **52**, 6930-6935.
35. C. X. Zu, Y. Z. Fu and A. Manthiram, *J Mater Chem A*, 2013, **1**, 10362-10367.
36. V. S. Kolosnitsyn, E. V. Kuzmina, E. V. Karaseva and S. E. Mochalov, *J Power Sources*, 2011, **196**, 1478-1482.

View Article Online
DOI: 10.1039/C6MH00043F

37. C. Barchasz, F. Molton, C. Duboc, J. C. Lepretre, S. Patoux and F. Alloin, *Anal Chem*, 2012, **84**, 3973-3980.
38. N. S. A. Manan, L. Aldous, Y. Alias, P. Murray, L. J. Yellowlees, M. C. Lagunas and C. Hardacre, *J Phys Chem B*, 2011, **115**, 13873-13879.
39. J. Wang, S. Y. Chew, Z. W. Zhao, S. Ashraf, D. Wexler, J. Chen, S. H. Ng, S. L. Chou and H. K. Liu, *Carbon*, 2008, **46**, 229-235.
40. L. X. Yuan, J. K. Feng, X. P. Ai, Y. L. Cao, S. L. Chen and H. X. Yang, *Electrochem Commun*, 2006, **8**, 610-614.

View Article Online
DOI: 10.1039/C6MH00043F

Suppression of the polysulfide-shuttle behavior in Li-S batteries through the development of a facile functional group on the polypropylene separator

Xingwen Yu, Jorphin Joseph, and Arumugam Manthiram*

A facile functional group developed on the polypropylene (PP) battery separator significantly suppresses the polysulfide-shuttle behavior in Li-S batteries.

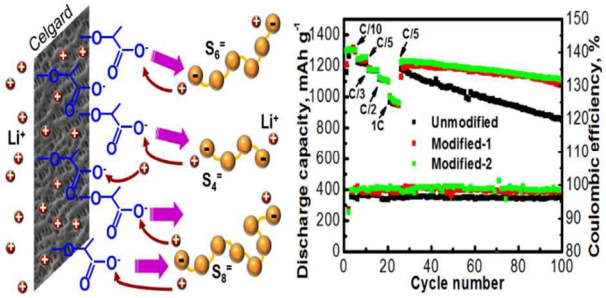

Journal of
Materials Chemistry A

Accepted Manuscript

This article can be cited before page numbers have been issued, to do this please use: X. Yu, J. Joseph and A. Manthiram, *J. Mater. Chem. A*, 2015, DOI: 10.1039/C5TA04289E.

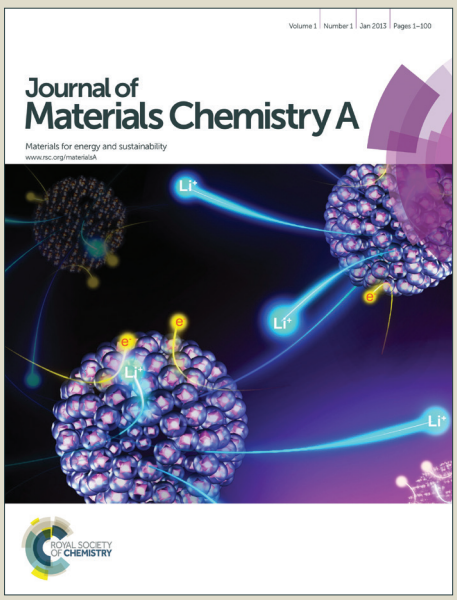

ROYAL SOCIETY OF CHEMISTRY

www.rsc.org/materialsA

View Article Online
DOI: 10.1039/C5TA04289E

Journal of Materials Chemistry A

ARTICLE

Polymer Lithium-Sulfur Batteries with a Nafion Membrane and an Advanced Sulfur Electrode†

Received 00th January 20xx,
Accepted 00th January 20xx

DOI: 10.1039/x0xx00000x

www.rsc.org/

Xingwen Yu, Jorphin Joseph and Arumugam Manthiram*

The development of lithium-sulfur (Li-S) battery technology is experiencing a critical challenge due to the migration of the soluble polysulfide species from the cathode to the lithium-metal anode which results in poor cyclability of the cell. To overcome the above issue, use of lithium-ion conductive membranes instead of the traditional porous Celgard membrane as the separator/electrolyte is one of the promising approaches. In this study, a lithiated Nafion membrane is used as a cation-selective electrolyte for Li-S batteries to suppress the polysulfide diffusion. An advanced cathode structure containing a high-surface activated carbon nanofiber (AC-CNF) current collector filled with dissolved lithium polysulfides and a thin AC-CNF upper current collector is used to improve the sulfur utilization. The Li-S battery system with the lithiated Nafion membrane and the sandwich cathode exhibits significantly enhanced cyclability relative to the cells with the traditional liquid-electrolyte integrated porous separator.

Introduction

The development of high-energy-density secondary battery technologies that can outperform the state-of-the-art Li-ion battery system is highly desired to meet the growing requirement of personal electronic devices, electric vehicles, and large-scale energy storage. In this regard, the battery system based on lithium–sulfur (Li-S) chemistries has attracted great interest in recent years as one of the top candidates for the next-generation energy storage technologies.[1-5] Due to the high intrinsic capacity of the sulfur cathode, the Li-S battery theoretically provides an energy density of 2600 W h kg^{-1},[6, 7] originating from the electrochemical redox reactions between the lithium metal and the elemental sulfur:[8]

$$nS + 2Li^+ + 2e^- \leftrightarrow Li_2S_n\ (4 \le n \le 8) \qquad E = 2.4 - 2.1\ V \qquad (1)$$

$$Li_2S_n + (2n\text{-}2)Li^+ + (2n\text{-}2)e^- \leftrightarrow nLi_2S\ (4 \le n \le 8) \quad E = 2.1 - 1.5\ V \quad (2)$$

Reaction (1) generates soluble lithium polysulfides (Li_2S_n, where $4 \le n \le 8$) and reaction (2) leads to the formation of insoluble lithium sulfide (Li_2S and/or Li_2S_2). Therefore, the electrochemical charge/discharge processes of a Li-S battery include a series of solid–liquid–solid transformations, which cause great complexity for Li-S battery systems.[8-12] Although the Li-S battery chemistry had been proposed for more than 30 years, implementation of this rechargeable battery technology is still hindered by some basic obstacles. One of the major obstacles for practical applications of Li-S batteries is caused by the soluble nature of the highly-ordered lithium polysulfides (Li_2S_n, $4 \le n \le 8$, intermediate charge/discharge products) in the organic electrolytes.[2, 10] During charge-discharge of the cell, the dissolved lithium polysulfides diffuse from the cathode to the lithium anode through the separator and induce a so-called "shuttle effect". Such shuttle effect causes the loss of the active sulfur materials and lowers the Coulombic efficiency of Li-S batteries.[11-17]

To overcome the above polysufide shuttling problem for the Li-S batteries, several strategies, including the confinement within micropores,[18, 19] hollow sphere structures,[20] conducting polymer coatings,[21, 22] and limitation of sulfur by covalent bonds within polymers,[23-26] polysulfide reservoirs[27], have been proposed to limit the diffusion of polysulfides. However, the use of liquid-electrolyte integrated porous separator was not able to fully address the polysulfide diffusion issue.

Cation-exchange polymer membranes have been used in various industry processes. One well-known example is the Nafion ionomer thin film, a copolymer of tetrafluoroethylene and perfluoro-vinyl-ether, which has been widely used in the proton exchange membrane fuel cells (PEMFCs) and chlorine-caustic soda industries due to its excellent stability and high proton conductivity.[28] When turning H^+ to Li^+ form, the Nafion polymer material has the ability to transfer Li^+.[29-35] The ionic conductivity and swelling behavior of lithiated Nafion ionomer, as well as its application in Li-ion batteries with metal oxide cathodes have been previously investigated.[29-31] Recently, two approaches involving the use of either a Nafion modified

Materials Science & Engineering Program and Texas Materials Institute, The University of Texas at Austin, Austin, TX78712, USA.
E-mail: manth@austin.utexas.edu

†Electronic Supplementary Information (ESI) available: Schematic of a setup for polysulfide permeation tests; SEM image of the as-prepared carbon nanofiber paper electrode; BET surface area and pore volume of the un-activated versus CO_2-activated CNF paper; Molecular structures of the original Nafion and lithiated Nafion materials; Pictures of fresh and cycled Nafion membranes; Charge/discharge profiles of the Li || Nafion / CNF interlayer || AC-CNF/lithium polysulfide batteries at different representative cycles at C/10, C/5, and C/3 rates. See DOI: 10.1039/x0xx00000x

porous Celgard separator or a lithiated free-standing Nafion ionomer film have been explored with Li-S batteries; they showed the advantage of the Nafion ionmer for suppressing the polysulfide diffusion.[32-35] In light of the above findings, we herein report a polymer Li-S battery by integrating a carbon-paper "interlayer" between the sulfur cathode and the lithiated polymer Nafion membrane electrolyte. The Nafion membrane was lithiated in the Li^+-containing organic electrolyte, which was used for cell assembly without any drying or other post-treatment processes. A light-weight, high-surface activated carbon nano-fiber (AC-CNF) paper electrode was used as a free-standing cathode matrix to accommodate the charge/discharge products and intermediates. The sulfur cathodes were prepared by dispersing the dissolved lithium polysulfide into the AC-CNF paper electrodes. A thin AC-CNF interlayer was also applied to the cell to suppress polysulfide diffusion and improve the cycling performance of the Li-S cell.

Experimental

Chemicals and materials

Dimethoxy ethane (DME, 99+ %, Acros Organics), 1, 3-dioxolane (DOL, 99.5 %, Acros Organics), lithium trifluoromethanesulfonate ($LiCF_3SO_3$, 98 %, Acros Organics), lithium nitrate ($LiNO_3$, 99+ %, Acros Organics), sublimed sulfur powder (99.5 %, Acros Organics), and lithium sulfide (Li_2S, 99.9 %, Acros Organics) were purchased and used as received. Carbon nanofiber (CNF, 50 - 200 μm long, ~ 100 nm diameter) powder possessing a "self-weaving" characteristics was purchased from Pyrograf Products Inc. (PR-24-XT-PS). Nafion 212 membrane was purchased from the Fuel Cell Stores.

Preparation and activation of free-standing, binder-free carbon nanofiber paper (CNF) electrodes and interlayers

Both the self-weaving, free-standing activated CNF electrodes and the interlayers were synthesized through a series of dispersion → vacuum filtration → peel off → vacuum drying → activation processes. For a typical synthesis, 380 mg of carbon nanofiber was dispersed in 500 mL of deionized water by high-power ultrasonication for 10 min with the addition of 25 mL of isopropyl alcohol (for wetting the surface of CNFs). The mixture was further vigorously stirred on a magnetic stirring plate for 2 h. Then, the products were collected on a piece of filter paper under vacuum and washed with de-ionized water, ethanol, and acetone several times. The free-standing CNF paper thus formed is a flexible film after drying for 24 h at 50 °C in a vacuum oven, which can be easily peeled off the filter paper. Finally, the CNF paper was punched out in circular disks with 1.2 cm diameter (1.13 cm^2) with ~ 6.8 mg mass.

Activation of the CNF paper was performed in a tube furnace by heating the as-obtained CNF paper at 875 ^oC for two hours under a flowing CO_2 atmosphere, as described in our previous paper.[36] Upon this activation process, the weight of the CNF paper electrode was reduced from ~ 6.8 mg to ~ 2.26 mg (~ 2.0 mg cm^{-2}). For the interlayer-structure cells, the weight of the AC-CNF paper electrode and the interlayer were adjusted by using different amounts of starting CNF powder materials to maintain a total carbon material (CNF cathode matrix and interlayer) at the cathode of ~ 2.0 mg cm^{-2}.

Synthesis of Li_2S_6 polysulfide catholyte

The lithium polysulfide catholyte was synthesized as we previously presented[37, 38] and is given below. A blank electrolyte was prepared by dissolving an appropriate amount of $LiCF_3SO_3$ and $LiNO_3$ in a DME/DOL (1 : 1 volume ratio) mixture solvent to render a 1.0 M $LiCF_3SO_3$ and 0.1 M $LiNO_3$ solution. To prepare the dissolved lithium polysulfide catholyte, sublimed sulfur powder and an appropriate amount of Li_2S were added to a proper amount of blank electrolyte to render 1.5 M sulfur in the stoichiometric form of Li_2S_6 in the solution. The mixture solution was heated at 50 °C in an Ar-filled glove box for 24 h to produce a dark purple solution with a moderate viscosity.

Lithiation of Nafion membrane

The Nafion membrane was soaked in the blank electrolyte comprising 1.0 M $LiCF_3SO_3$ and 0.1 M $LiNO_3$ in the DME/DOL (1 : 1, volume ratio) solvent for 7 days. The lithiated Nafion membrane was then used for cell assembly without any further drying or post-treatment process.

Cell assembly

The Li || Nafion || AC-CNF/lithium polysulfide cells were assembled with CR2032 coin cell configuration in an Ar-filled glove box. First, 40 μL of lithium polysulfide catholyte was added into the activated AC-CNF paper electrode. Then, a lithiated Nafion membrane was placed on top of the AC-CNF electrode. Another 40 μL of blank electrolyte was added onto the Nafion membrane. Finally, the lithium-metal foil anode was placed on the Nafion membrane. Then, the coin cell was sealed inside the glove box. For the assembly of the cells with the AC-CNF interlayer, a piece of ultra-thin AC-CNF paper was pre-attached to the lithiated Nafion membrane on the side to be facing the cathode. In this case, the mass ratio of the cathode matrix to the interlayer was 3 : 1. The rest of the assembly procedures are the same as indicated above.

Electrochemical characterization

For the battery cycling measurements, the cells were galvanostatically charged and discharged at different C-rates with an Arbin® battery test station. The capacity values shown in this paper were calculated based on the mass of the active sulfur materials within the electrodes. Cyclic voltammetry data were collected with a VoltaLab PGZ402 potentiostat at 0.1 mV s^{-1}. The ionic conductivity of the lithiated Nafion membrane was determined with the conventional AC impedance method with two electrodes. Impedance was measured with a Solartron 1287 potentialstat, employing two blocking stainless steel electrodes in the frequency range of 1 MHz to 0.1 Hz.

Characterization

Morphological characterizations were carried out with a FEI Quanta 650 scanning electron microscope (SEM). The

View Article Online
DOI: 10.1039/C5TA04290E

elemental mapping results were examined with an energy dispersive spectroscometer (EDS) attached to the FEI Quanta 650 SEM. Samples of the cycled cells for SEM analyses were collected by opening the cells inside the Ar-filled glove box. Attenuated total reflectance Fourier transform infrared spectroscopy (ATR-FTIR) experiments were performed with a Nicolet IS5 FTIR spectrometer.

Polysulfide diffusion measurements

Permeation of the lithium polysulfide catholyte through the Celgard separator or the lithiated Nafion membrane was optically tested with a setup shown in Fig. S1a-d. Thereby, a 4.0 mL solution of 0.25 M Li_2S_6 (nominal concentration) in DME/DOL (1 : 1 volume ratio) was placed inside a transparent tube, whereas the opposite side of the separator was filled with the pristine DME/DOL (1 : 1 volume ratio) solvent. During the experiment, the solutions rested without movement to exclude external influence on the diffusion test of polysulfides through the membranes. The resulting color change was evaluated by visual examination.

Results and discussion

Cell configuration and material characterizations

The battery configuration of a Li-S cells in this study is displayed in Fig. 1a, in which a lithiated polymer Nafion membrane serves both as a Li^+-ion conductive electrolyte and as an electrically non-conductive separator. A piece of AC-CNF interlayer was placed between the lithium polysulfide cathode and the lithiated polymer membrane. Fig. 1b shows the attenuated total reflectance Fourier transform infrared spectra (ATR-FTIR) of the untreated versus lithiated Nafion membranes. The symmetric stretching vibrations of S-O bond considerably changes in the Nafion membrane upon lithiation (shifts from 1050 cm^{-1} to 1070 cm^{-1}). A concerted shift is observed for the peaks at 1700 cm^{-1} to 1650 cm^{-1} when the counter ion is changed to lithium, which is consistent with the lithiation characteristics in the previous relevant studies.[32-35] The disappearance of the weak peak at 924 cm^{-1} further confirmed the exchange of H^+ with Li^+.[32-35] Upon saturation with the $LiCF_3SO_3$-DME/DOL electrolyte, the size of the membrane expanded by ~ 1.2 times. Due to the absorption of the blank electrolyte into the membrane, quantification of the conversion of H^+ to Li^+ in the Nafion molecules is currently difficult to be precisely determined. The peak shift in the FTIR spectra qualitatively reveals the lithiation after the electrolyte-soaking process. Replacement of H^+ with Li^+ may also occur during electrochemical cycling of the cells. A detailed mechanistic study of the lithiation process of Nafion membrane will be performed with both *in-situ* and *ex-situ* methodologies in the future. In comparison to the previous lithiation methods performed in aqueous solutions, the lithiation approach in this study is relatively simple; more importantly, it also avoids the possibility of any deformation of the membrane during drying process. In addition, it avoids any possible concerns about water contamination to the Li-S cells due to the insufficient drying. Furthermore, since size expansion of the membrane has occurred before cell assembly, the deformation due to the membrane swelling can be avoided during cell cycling. From an electrochemical impedance spectroscopic (EIS) analysis, the ionic conductivity of the lithiated Nafion membrane is ~ 1.0×10^{-5} S. cm^{-1}. Fig. 1c shows the SEM image of the activated AC-CNF paper electrode. With a single fiber diameter of ~ 100 nm, the interwoven CNF fabric has micron-sized interspaces. In comparison to the as-prepared CNF paper (Fig. S2), the CO_2-activated CNF does not show significant structure change from the SEM images. However, from our previous Brunauer–Emmett–Teller (BET) analyses,[36] both the BET surface and the pore volume of the CNF materials had been greatly enhanced upon the CO_2-activation treatment (Table S1). Furthermore, the BET analyses also indicated the coexistence of micro-, meso-, and macro-pores in the CO_2-activated CNF electrode,[36] which was a facile structure for effectively trapping the dissolved polysulfides and accommodating the charge/discharge products of the Li-S battery.

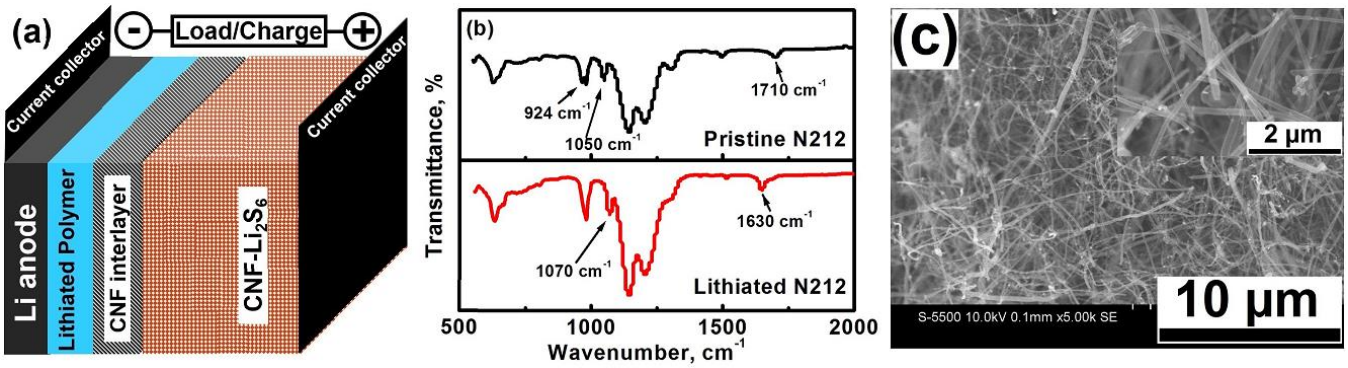

Fig. 1. (a) Schematic of a lithium-dissolved polysulfide battery with a lithiated Nafion membrane as the Li^+-ion selective electrolyte/separator. The cathode contains a high-surface activated carbon nanofiber (AC-CNF) current collector filled with dissolved lithium polysulfides and a thin AC-CNF interlayer/upper current collector between the polysulfide cathode and the lithiated Nafion membrane. (b) Attenuated total reflectance Fourier transform infrared spectroscopy (ATR-FTIR) of an untreated versus a lithiated Nafion membrane. (c) Scanning electron microscopy (SEM) image of the freshly prepared CO_2-activated CNF free-standing paper electrode.

View Article Online
DOI: 10.1039/C5TA04285E

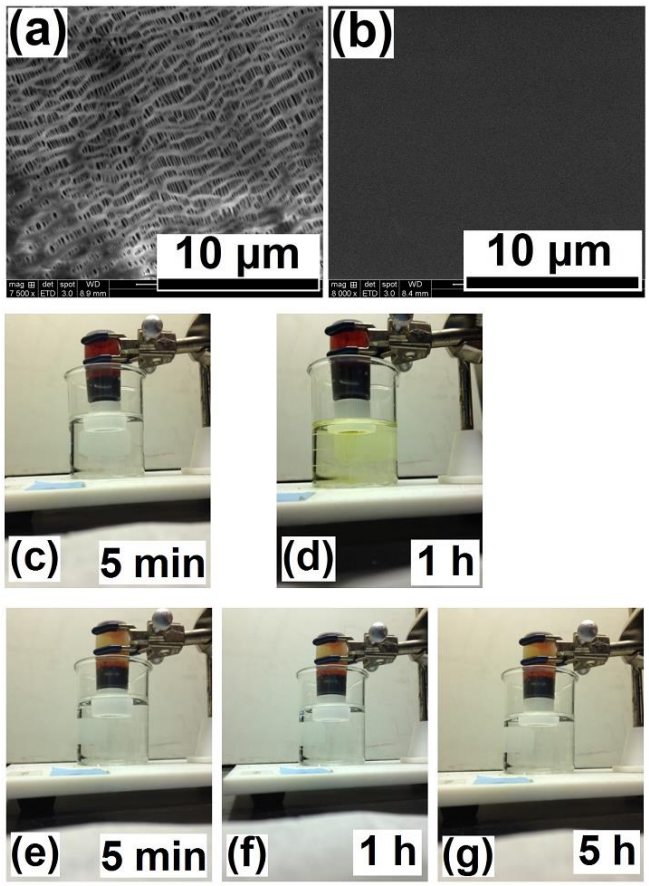

Fig. 2. (a) SEM image of a porous Celgard separator. (b) SEM image of a Nafion membrane. (c)-(d) Polysulfide diffusion test of the Celgard separator after various resting times. (e)-(g) Polysulfide diffusion test of the lithiated Nafion membrane after various resting times.

Suppression of polysulfide permeation by the lithiated Nafion membrane

Fig. 2a and b compare the SEM morphologies of the lithiated Nafion membrane and the Celgard separator, which was commonly used in the Li^+-ion and Li-S battery research. The Celgard membrane shows a porous structure with pore dimensions in the µm-scale, which unavoidably allows the migration of the dissolved lithium polysulfide species from the cathode to the lithium-metal anode. However, as seen in Fig. 2b, the lithiated Nafion membrane shows a dense, uniform morphology, which is supposed to not allow the migration of the dissolved lithium polysulfide species. In order to evaluate the advantage of the non-porous lithiated Nafion membrane for retention of dissolved lithium polysulfide species, a series of simple, but informative polysulfide diffusion measurements were performed with the setup schematized/pictured in Fig. S1. The test procedures were as detailed in the experimental section. As was predicted, the porous Celgard separator did not suppress the diffusion of polysulfides, thus the colour of the DME/DOL solution is changed from colourless to light yellow after ~ 1 h of rest due to the diffusion of long chain polysulfides from the reservoir through the Celgard separator. (Fig. 2c, d). In contrast, the lithiated Nafion membrane effectively suppressed the diffusion of polysulfide species. After 5 h of rest, no colour change of the DME/DOL solvent was observed (Fig. 2e-g). It should be noted that the thickness of the Celgard separator and the Nafion membrane used here are, respectively, 25 µm and 50 µm. In order to confirm that the polysulfide retention effect is not due to the thickness of the Nafion membrane, cells with multi-layer Celgard separators (two or even three layers) were tested with the same procedure as above. However, the multiple-layered Celgard separators did not provide any obvious improvement to prevent the polysulfide diffusion.

Electrochemical cycling performances of Li-S batteries with the lithiated Nafion membrane:

The Li-S batteries in this study were prepared with the lithium polysulfide as the starting active cathode material. Therefore, after the assembly, the cell was in a half charge/discharge state (usually with an open-circuit voltage of approximately 2.30 V), which can either be first charged or first discharged. In order to compare the cell performances at consistent cycling conditions, all the cells were first discharged in this study, Fig. 3a shows a typical voltage profile of a Li || Nafion || AC-CNF/lithium polysulfide cell. The initial discharge curve shows the characteristics of the conversion of long-chain lithium polysulfide into short-chain lithium polysulfide or lithium sulfide. The subsequent charge-discharge curves show the characteristic profiles of the regular Li-S batteries. Fig. 3b shows the cyclic voltammograms of the Li || Nafion || AC-CNF/lithium polysulfide cell. The potential was initially swept from the open-circuit voltage (OCV) to 1.6 V, followed by a positive sweep to 2.8 V at a rate of 0.1 mV s^{-1}. Then, 10 full cycles were performed between 2.8 and 1.6 V (the 1st, 2nd, 5th and 10th cycle are shown here as representatives). There are two cathodic peaks at ~ 2.3 V and ~ 1.85 V, corresponding to the reduction reactions of elemental sulfur and high-order polysulfides, and a broad anodic peaks in the anodic sweep, which indicate the staged transition of short-chain lithium polysulfide (*e.g.*, Li_2S_2) or lihtium sulfide (Li_2S) to long-chain lithium polysulfides (*e.g.*, Na_2S_n $4 \leq n \leq 8$) to elemental sulfur.[16] The distinguishably broad cathodic curve in the first cycle is presumed to be attributed to the prolonged conditioning of the cell. In the following cycles, the sharp cathodic and anodic peaks display no significant peak intensity and potential changes, which indicates an electrochemically stable environment within the AC-CNF/lithium polysulfide cathodes. This results in good reversibility of the reduction/oxidation reactions of the sulfur ↔ long-chain polysulfides ↔ short-chain polysulfides ↔ sulfide during repeated cycling process.

Rate capabilities of the Li || Nafion || AC-CNF/lithium polysulfide cells were tested at C/10, C/5, C/3, and C/2 rates. Representative charge/discharge profiles at the 5th cycle of each cell at different C-rates are displayed in Fig. 3c. Both the charge and discharge curves show the clear two-voltage plateaus, indicating a favourable electrochemical environment in which the cathode and anode reactions occur. The cells exhibit high discharge capacities (based on the sulfur active mass within the catholyte) of ~ 1150, ~ 1100, ~ 1000, and ~

View Article Online
DOI: 10.1039/C5TA04239E

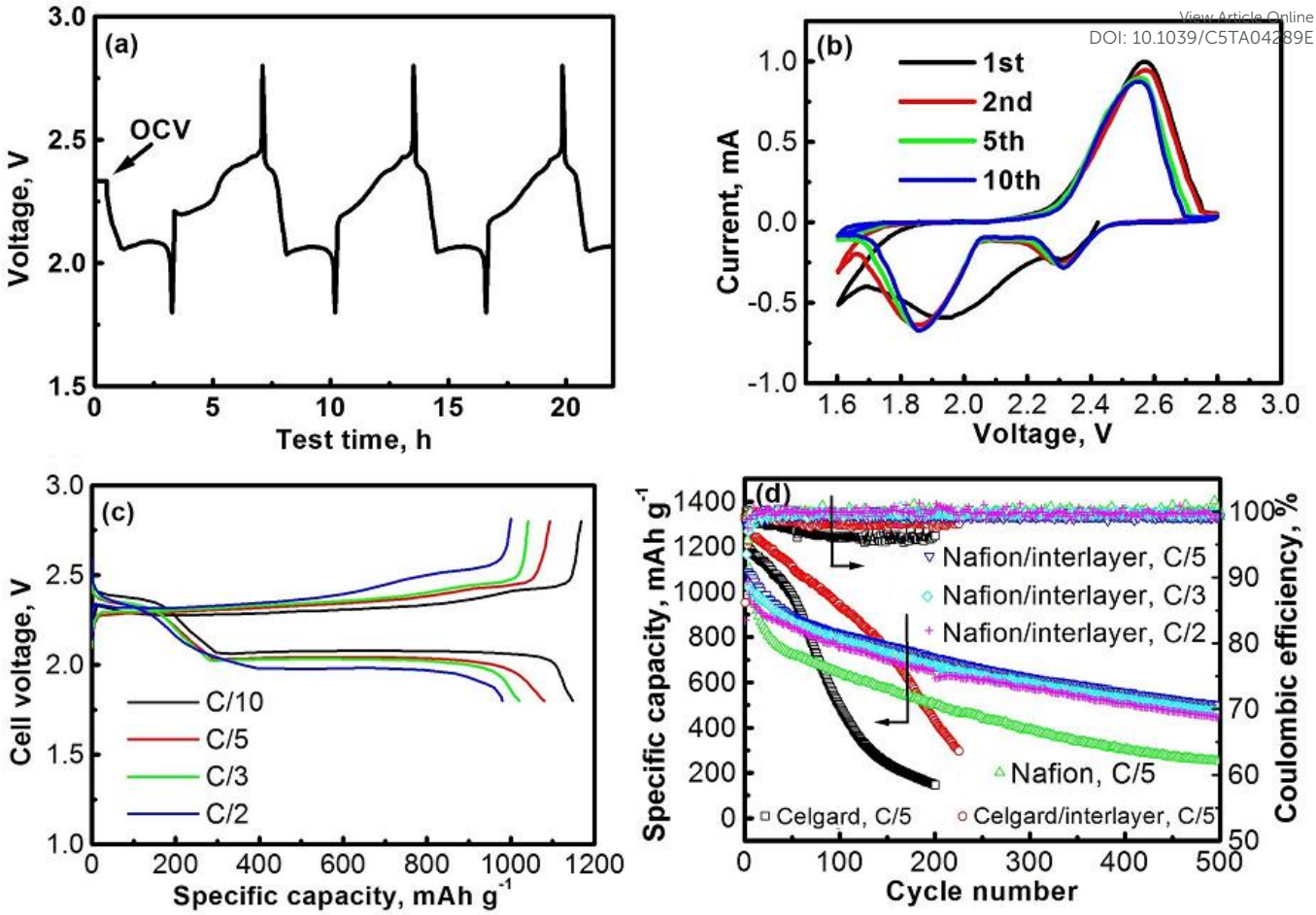

Fig. 3. (a) Voltage vs. time profile of the initial discharge and the following charge-discharge of a Li || Nafion || AC-CNF/lithium polysulfide cell at C/5 rate. (b) Cyclic voltammograms of a Li || Nafion || AC-CNF/lithium polysulfide cell at a scan rate of 0.1 mV s^{-1}. (c) Charge/discharge profiles of the Li || Nafion || AC-CNF/lithium polysulfide cells at different C-rates. (d) Discharge capacities and Coulombic efficiencies as a function of cycle number of a Li || Celgard || AC-CNF/lithium polysulfide cell, a Li || AC-CNF-interlayered Celgard || AC-CNF/lithium polysulfide cell, a Li || Nafion || AC-CNF/lithium polysulfide cell, and the Li || AC-CNF-interlayered Nafion || AC-CNF/lithium polysulfide cells at different C-rates.

950 mAh g^{-1} respectively, at C/10, C/5, C/3, and C/2 rates. The capacities obtained correspond to the transfer of *ca.* 1.4, 1.3, 1.2, and 1.1 electrons per sulfur atom respectively at C/10, C/5, C/3, and C/2 rates. The cells show increasing polarization behaviour as the cycling rate increases, which might be mainly due to the poor conductivity of the short-chain lithium polysulfide and/or lithium sulfide.

The lithiated Nafion membrane in Li-S cells in this study plays a "bi-functional" role, as both a Li^+-ion exchange electrolyte and as a non-electrically conductive separator. When turning the SO_3H^+ group to SO_3Li^+ form (as expressed in Fig. S3), the co-polymer of tetrafluoroethylene and perfluoro-vinyl-ether has the ability to transfer Li^+ cation as having been proved in Li-ion and Li-S battery research.[32-35] In the soluble polysulfide involved Li-S batteries, use of the non-porous lithiated Nafion membrane provides advantages over the traditional porous separators for suppressing the lithium-polysulfide anions from transporting through. Enhancement in the cyclability of the Li-S batteries on employing the lithiated Nafion membrane can be observed in Fig. 3d. The Li || Celgard || AC-CNF/lithium polysulfide cell with the porous Celgard membrane shows a higher initial discharge capacity than the Li || Nafion || AC-CNF/lithium polysulfide cell due to the fast ionic transport in the liquid electrolyte integrated Celgard membrane. However, degradation in the discharge capacity of the cell with the Celgard separator becomes faster after ~ 70 cycles, caused by the polysulfide shuttle behavior through the porous Celgard membrane. ~ 90 cycles later, the discharge capacities of the Li || Nafion || AC-CNF/lithium polysulfide cell exceed that of the cell with the Celgard separator. Noticeably, the cell with the lithiated Nafion membrane shows higher Coulombic efficiency than that with the Celgard membrane, further evidencing the advantage of the non-porous lithiated Nafion membrane for the suppression of polysulfide shuttling.

We have previously developed and systematically studied an interlayer-strategy for cyclability enhancement of the Li-S batteries by application of a carbon-based interlayer between the sulfur cathode and the porous Celgard separator.[39-42] In this study, for example, as seen in Fig. 3d, the cycling life of the Li || Celgard || AC-CNF/lithium polysulfide cell was

View Article Online
DOI: 10.1039/C5TA04289E

significantly improved by inserting an activated CNF interlayer between the Celgard and the polysulfide cathode. Herein, the interlayer-strategy was further investigated for the Li || Nafion || AC-CNF/lithium polysulfide batteries by inserting a thin activated CNF interlayer between the lithium polysulfide cathode and the Nafion membrane. Application of such an activated CNF interlayer to the Li || Nafion || AC-CNF/lithium polysulfide cells further improves their cyclability. As seen in Fig. 3d, the capacity after the initial few cycles increases by nearly 25% upon application of the AC-CNF interlayer to the Li || Nafion || AC-CNF/lithium polysulfide cell. The Li || Nafion / AC-CNF interlayer || AC-CNF/lithium polysulfide cells also exhibit excellent rate cyclability. After 500 cycles, the reversible capacities of the activated CNF-interlayered cells with the lithiated Nafion membranes remain at about 500, 470, and 450 mAh g^{-1} respectively at C/5, C/3, and C/2 rates.

Post-mortem analyses of the Li || Nafion / AC-CNF interlayer || AC-CNF/lithium polysulfide cells after cycling

Fig. 4a shows a SEM image of the discharged activated CNF cathode after 100 cycles. In comparison to the pristine activated CNF electrode (Fig. 1c), the interspaces of the activated CNF network are filled with discharged products and lithium salts. But the activated CNF electrode maintains its structure after cycling. The sulfur is uniformly distributed in the electrode, as indicated by the elemental mapping (Fig. 4b and c). Fig. 4d, e, and f show, respectively, the SEM image and EDS elemental mappings of carbon and sulfur for the activated CNF interlayer after 100 cycles. Comparison of Fig. 4a and 4d indicates that the discharge products are relatively less in the interlayer, which is further confirmed on comparing Fig. 4b, c with Fig. 4e, f. Either the discharge products in the AC-CNF cathode matrix or the trapped polysulfide species in the interlayer may sit within the 3D interwoven fibers or cover on the surface of the fibers. Therefore, according to the elemental mapping results (Fig. b, c, e, and f), the relatively higher carbon signal and relatively lower sulfur signal in the interlayer (Fig. 4e and f) indicates that most of the discharge products remain in the cathode matrix, but some dissolved polysulfide species may diffuse into the interlayer during cycling. As we have previously proposed,[39-42] the interlayer in a Li-S battery generally plays two major roles: (1) the 3-dimensional nano-framework and tortuous interspace of the interlayer can trap the long-chain soluble lithium polysulfide species and prevent/alleviate their migration to the anode, and (2) the carbon-based interlayer is electrically conductive and acts as a secondary current collector to capture and retain the polysulfide species by electrochemical deposition of the sulfur/sulfides. Therefore, some trapped polysulfide species in the interlayer may also be oxidized to sulfur during charge, and be reduced to lithium sulfide during discharge. The above two

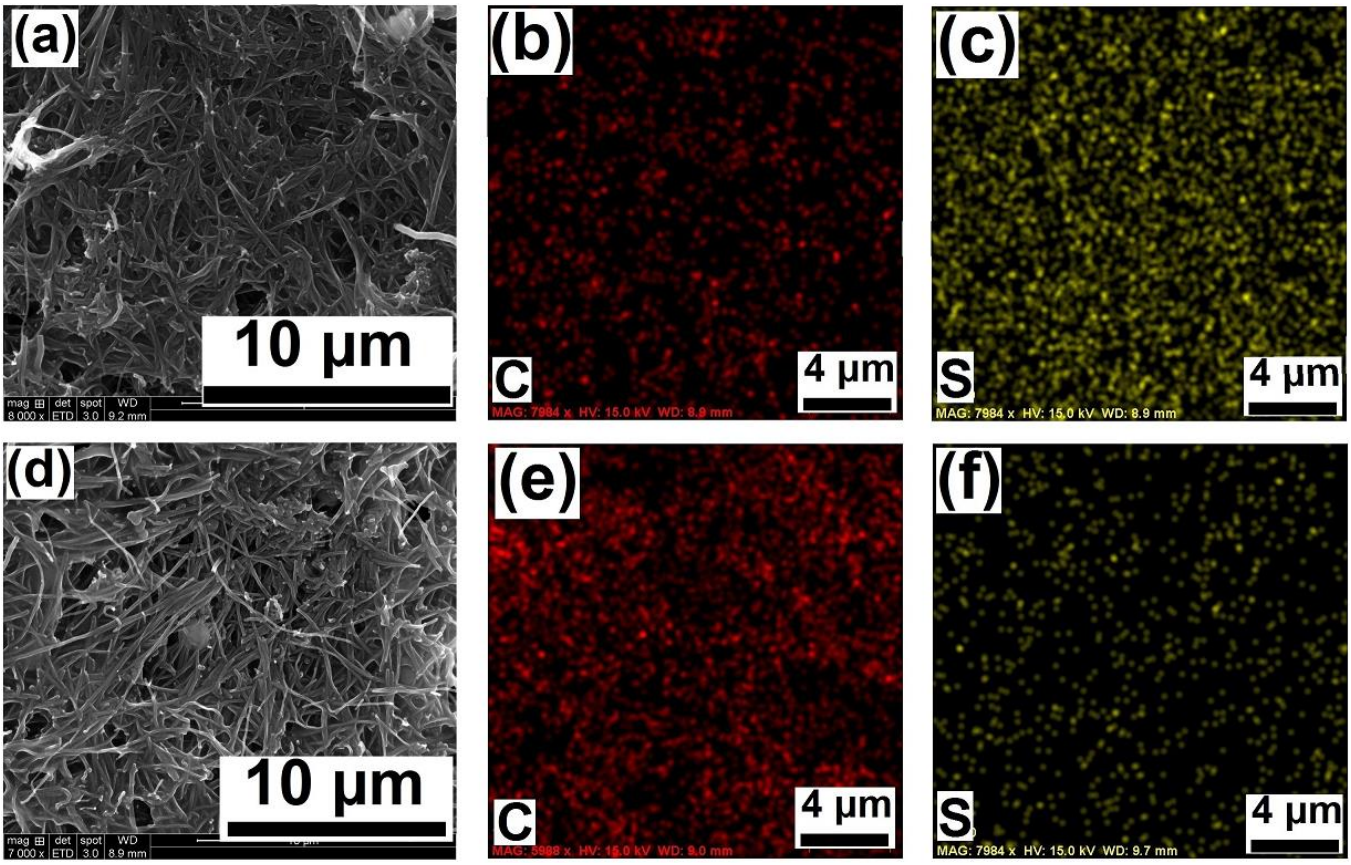

Fig. 4. (a) SEM image of the activated CNF cathode matrix after 100 cycles. (b) Carbon and (c) sulfur elemental mappings of the cycled (after 100 times) activated CNF cathode matrix obtained with EDS. (d) SEM image of the activated CNF interlayer after 100 cycles. (e) Carbon and (f) sulfur elemental mappings of the cycled (after 100 times) AC-CNF interlayer obtained with EDS.

functions of the interlayer effectively alleviates the migration of the dissolved polysulfides from the cathode to the anode and significantly improves the cycle life of the Li-S batteries, as evidenced in Fig. 3d. However, with the prolonging of the cycling, the diffusing of the soluble polysulfides may also reach the interface between the interlayer and the separator. In such case, if a porous separator is applied in the cell (such as the cells with Celgard separator), the soluble polysulfides may also possibly diffuse through the pores of the separator to the anode and induces the "polysulfide shuttle" effects. However, if a separator, such as lithiated Nafion membrane is used, the "polysulfide shuttle" effects could be completely prevented. Therefore, the cells with the lithiated Nafion membrane showed significant benefits in terms of the cycle life of the cells (Fig. 3d). The second role of the interlayer acting as the secondary current collector is also important for the Li-S batteries. It provides an electrochemical environment for the diffusing or trapped polysulfides to be involved in the redox reactions. In addition, the interlayer is also able to accommodate some of the stress and volume expansion during the discharge of sulfur and endure the volume changes of the trapped active material during cycling. Therefore, the sulfur utilization of the activated CNF-interlayered cells either with the Celgard membrane or with the lithiated Nafion membrane show higher discharge capacities relative to the non-interlayered cells throughout the cycling (Fig. 3d).

Fig. 5a, b, and c, respectively, show the surface morphologies of the pristine and cycled lithium anodes taken out of the cells either with the lithiated Nafion membrane or with the Celgard membrane. In comparison to the fresh Li metal, the surfaces of the lithium anodes become severely rough after cycling (100 cycles), especially for the one in the cell with the Celgard separator (Fig. 5c). Surface changes at the Li-metal anode may be one of the major issues that are responsible for the capacity fade of the Li-S cells during cycling. EDS analyses of the cycled Li anodes are displayed in Fig. 5d and e. The sulfur signal is evidently higher in the Li anode in the cell with the Celgard separator than that in the cell with the lithiated Nafion membrane, implying the diffusion of the polysulfide species through the porous Celgard separator during cell cycling. The sulfur signal of the Li-metal anode in the cell with the lithiated Nafion membrane may result from the $LiCF_3SO_3$ salt in the electrolyte or a small amount of polysulfide diffusion. The Nafion membrane maintained a good shape after electrochemical cycling of the cell (as seen in Fig. S4), indicating a good compatibility between the Nafion membrane and the liquid electrolyte and lithium polysulfides. ATR-FTIR analysis of the cycled Nafion membrane is presented in Fig. 5f, which shows the same characteristics as the lithiated Nafion membrane before cycling (Fig. 1b). Fig. S5 compare the voltage profiles of the Li || Nafion / CNF interlayer || AC-CNF/lithium polysulfide cells at different cycles. No significant

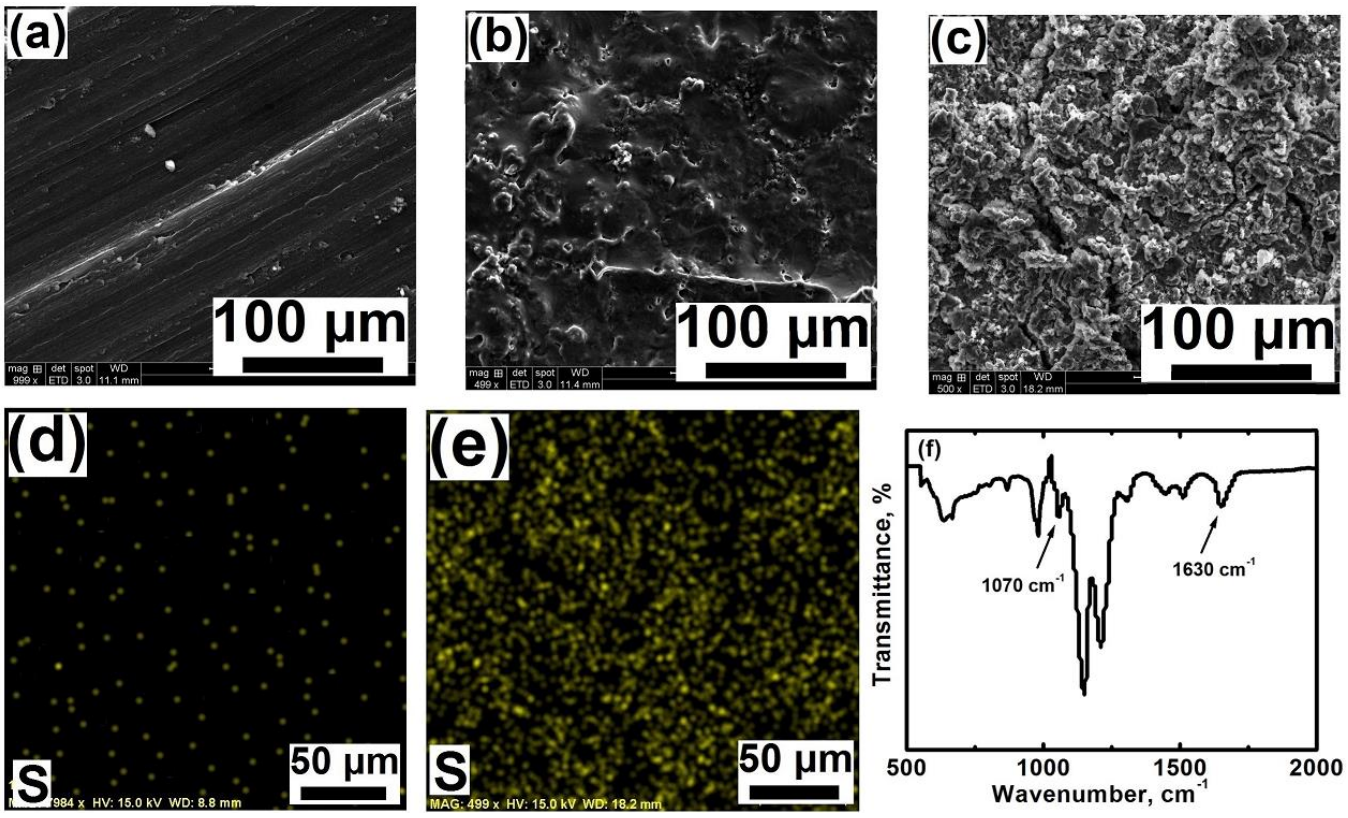

Fig. 5. (a) SEM image of a fresh Li anode. (b) SEM image of a Li anode in a Li || AC-CNF-interlayered Nafion || AC-CNF/lithium polysulfide cell after 100 cycles. (c) SEM image of a Li anode in a Li || Celgard || AC-CNF/lithium polysulfide cell after 100 cycles. (d) EDS elemental (sulfur) mapping of the Li anode in the Li || AC-CNF-interlayered Nafion || AC-CNF/lithium polysulfide cell after 100 cycles. (e) EDS elemental (sulfur) mapping of the Li anode in the Li || Celgard || AC-CNF/lithium polysulfide cell after 100 cycles. (f) ATR-FTIR spectrum of the Nafion membrane in the Li || AC-CNF-interlayered Nafion || AC-CNF/lithium polysulfide cell after 100 cycles.

View Article Online
DOI: 10.1039/C5TA04289E

increase in polarization is observed during cycling at different C-rates. The voltage gaps between the charge and the discharge curves did not significantly increase with prolonged cycling. This observation is in agreement with the EIS analysis that the cycled Nafion membrane maintained the same ionic conductivity as the freshly lithiated membranes. From the above analyses, the capacity fade of the cells with the lithiated Nafion membrane may majorly attributed to the degradation of the Li-metal anode surface. Detailed understanding of the degradation mechanism of the lithium anode, as well as the Li-anode protection will be one of our research emphases in the future.

According to the results we obtained so far, the benefits of using the lithiated Nafion membrane have been demonstrated by (1) the polysulfide diffusion test (Fig. 2), (2) electrochemical characterizations (Fig. 3), and (3) SEM/EDS analysis of the cycled lithium-anode (Fig. 5). Our on-going and future work with the Nafion membrane approach includes a series of applied research as well as a deep insight into the mechanistic investigations. Since the Nafion membrane effectively supressed the migration of the lithium polysulfide from the cathode to the anode, the electrolyte additive $LiNO_3$ might not be necessary in the Li-S batteries (need to be confirmed in the future). In addition to the structural effect (non-porous characteristics relative to the Celgard separator, as compared in Fig. 2a and b), physico-chemical, electrochemical, and/or electronic interactions between the polysulfide species (with different order-level) and the functional groups of the Nafion molecules (including the polytetrafluoroethylene backbone, perfluoro-vinyl-ether group, and sulfonic acid functional group) may play important roles for hindering the shuttling of the polysulfides. In addition, the lithiation mechanism (conversion of H^+ with Li^+) of the Nafion membrane in the organic electrolyte under special chemical and/or electrochemical conditions will be an interesting and important aspect for further detailed investigation.

Conclusions

We presented a lithium-sulfur cell with a lithiated Nafion membrane as the Li^+-ion selective separator/electrolyte, and a dissolved lithium polysulfide dispersed into a light-weight activated carbon nanofiber paper (AC-CNF) as the cathode. The non-porous lithiated Nafion membrane provides both acceptable lithium-ion conductivity and significantly reduced lithium polysulfide permeation, demonstrating significant advantages over the porous Celgard separators in terms of suppressing soluble polysulfide migration and cycle-life for Li-S batteries. The binder-free, light-weight activated CNF paper electrode offers both a robust structure for the electrode with the interwoven CNF fiber and high accommodation ability for the cycling products with the high-surface-area and the interspaces of the CNF fabrics. Integration of an activated carbon nanofiber interlayer between the polysulfide cathode and the lithiated Nafion membrane further improves the performances of the cell. The Li || interlayered Nafion || AC-CNF/lithium polysulfide cells exhibit remarkably high capacity density and cycling stability.

Acknowledgements

This work was funded in part by the Advanced Research Projects Agency-Energy (ARPA-E), U.S. Department of Energy, under Award Number DE-AR0000377. One of the authors (J. J.) thanks the University Grants Commission (UGC), India, for the award of a Raman Postdoctoral Fellowship.

References

1 A. Manthiram, S. H. Chung and C. X. Zu, *Adv. Mater.*, 2015, **27**, 1980-2006.
2 A. Manthiram, Y. Z. Fu, S. H. Chung, C. X. Zu and Y. S. Su, *Chem. Rev.*, 2014, **114**, 11751-11787.
3 A. Manthiram, Y. Z. Fu and Y. S. Su, *Accounts Chem. Res.*, 2013, **46**, 1125-1134.
4 L. F. Nazar, M. Cuisinier and Q. Pang, *MRS Bull.*, 2014, **39**, 436-442.
5 Y. X. Yin, S. Xin, Y. G. Guo and L. J. Wan, *Angew. Chem. Int. Ed.*, 2013, **52**, 13186-13200.
6 Z. Yuan, H. J. Peng, J. Q. Huang, X. Y. Liu, D. W. Wang, X. B. Cheng and Q. Zhang, *Adv. Funct. Mater.*, 2014, **24**, 6105-6112.
7 M. Q. Zhao, H. J. Peng, G. L. Tian, Q. Zhang, J. Q. Huang, X. B. Cheng, C. Tang and F. Wei, *Adv. Mater.*, 2014, **26**, 7051-7058.
8 C. Barchasz, F. Molton, C. Duboc, J. C. Lepretre, S. Patoux and F. Alloin, *Anal. Chem.*, 2012, **84**, 3973-3980.
9 Y. S. Su, Y. Z. Fu, T. Cochell and A. Manthiram, *Nat. Commun.*, 2013, **4**, 2985.
10 G. Y. Xu, B. Ding, J. Pan, P. Nie, L. F. Shen and X. G. Zhang, *J. Mater. Chem. A*, 2014, **2**, 12662-12676.
11 Q. Wang, J. M. Zheng, E. Walter, H. L. Pan, D. P. Lv, P. J. Zuo, H. H. Chen, Z. D. Deng, B. Y. Liaw, X. Q. Yu, X. Q. Yang, J. G. Zhang, J. Liu and J. Xiao, *J. Electrochem. Soc.*, 2015, **162**, A474-A478.
12 C. X. Zu and A. Manthiram, *Adv. Energy Mater.*, 2014, **4**, 1400897.
13 S. H. Chung and A. Manthiram, *Adv. Mater.*, 2014, **26**, 7352-7357.
14 S. H. Chung and A. Manthiram, *Adv. Funct. Mater.*, 2014, **24**, 5299-5306.
15 Y. Z. Fu, C. X. Zu and A. Manthiram, *J. Am. Chem. Soc.*, 2013, **135**, 18044-18047.
16 S. H. Chung and A. Manthiram, *Electrochim. Acta*, 2013, **107**, 569-576.
17 Y. S. Su, Y. Z. Fu, B. K. Guo, S. Dai and A. Manthiram, *Chem.-Eur. J.*, 2013, **19**, 8621-8626.
18 J. X. Song, T. Xu, M. L. Gordin, P. Y. Zhu, D. P. Lv, Y. B. Jiang, Y. S. Chen, Y. H. Duan and D. H. Wang, *Adv. Funct. Mater.*, 2014, **24**, 1243-1250.
19 T. Xu, J. X. Song, M. L. Gordin, H. Sohn, Z. X. Yu, S. R. Chen and D. H. Wang, *ACS Appl. Mater. Inter.*, 2013, **5**, 11355-11362.
20 C. F. Zhang, H. B. Wu, C. Z. Yuan, Z. P. Guo and X. W. Lou, *Angew. Chem. Int. Ed.*, 2012, **51**, 9592-9595.
21 Y. Yang, G. H. Yu, J. J. Cha, H. Wu, M. Vosgueritchian, Y. Yao, Z. A. Bao and Y. Cui, *ACS Nano*, 2011, **5**, 9187-9193.
22 G. Q. Ma, Z. Y. Wen, J. Jin, Y. Lu, K. Rui, X. W. Wu, M. F. Wu and J. C. Zhang, *J. Power Sources*, 2014, **254**, 353-359.
23 L. Wang, Z. H. Dong, D. Wang, F. X. Zhang and J. Jin, *Nano Lett.*, 2013, **13**, 6244-6250.

Journal of Materials Chemistry A ARTICLE

View Article Online
DOI: 10.1039/C5TA04289E

24 Y. Z. Fu and A. Manthiram, *Chem. Mater.*, 2012, **24**, 3081-3087.
25 Y. Z. Fu and A. Manthiram, *J. Phys. Chem. C*, 2012, **116**, 8910-8915.
26 Y. Z. Fu, Y. S. Su and A. Manthiram, *ACS Appl. Mater. Inter.*, 2012, **4**, 6046-6052.
27 X. L. Ji, S. Evers, R. Black and L. F. Nazar, *Nat Commun*, 2011, **2**.
28 Y. Wang, K. S. Chen, J. Mishler, S. C. Cho and X. C. Adroher, *Appl. Energy*, 2011, **88**, 981-1007.
29 H. Y. Liang, X. P. Qiu, S. C. Zhang, W. T. Zhu and L. Q. Chen, *J. Appl. Electrochem.*, 2004, **34**, 1211-1214.
30 R. R. Garsuch, D. B. Le, A. Garsuch, J. Li, S. Wang, A. Farooq and J. R. Dahn, *J. Electrochem. Soc.*, 2008, **155**, A721-A724.
31 M. K. Wang, F. Zhao and S. J. Dong, *J. Phys. Chem. B*, 2004, **108**, 1365-1370.
32 I. Bauer, S. Thieme, J. Bruckner, H. Althues and S. Kaskel, *J. Power Sources*, 2014, **251**, 417-422.
33 Q. W. Tang, Z. Q. Shan, L. Wang, X. Qin, K. L. Zhu, J. H. Tian and X. S. Liu, *J. Power Sources*, 2014, **246**, 253-259.
34 Z. Q. Jin, K. Xie, X. B. Hong, Z. Q. Hu and X. Liu, *J. Power Sources*, 2012, **218**, 163-167.
35 J. Q. Huang, Q. Zhang, H. J. Peng, X. Y. Liu, W. Z. Qian and F. Wei, *Energy Environ. Sci.*, 2014, **7**, 347-353.
36 L. Qie and A. Manthiram, *Adv. Mater.*, 2015, **27**, 1694-1700.
37 X. W. Yu and A. Manthiram, *Phys. Chem. Chem. Phys.*, 2015, **17**, 2127-2136.
38 Y. Z. Fu, Y. S. Su and A. Manthiram, *Angew. Chem. Int. Ed.*, 2013, **52**, 6930-6935.
39 S. H. Chung and A. Manthiram, *Chem. Commun.*, 2014, **50**, 4184-4187.
40 R. Singhal, S. H. Chung, A. Manthiram and V. Kalra, *J. Mater. Chem. A*, 2015, **3**, 4530-4538.
41 Y. S. Su and A. Manthiram, *Nat. Commun.*, 2012, **3**, 1166.
42 C. X. Zu, Y. S. Su, Y. Z. Fu and A. Manthiram, *Phys. Chem. Chem. Phys.*, 2013, **15**, 2291-2297.

View Article Online
DOI: 10.1039/C5TA04289E

Polymer Lithium-Sulfur Batteries with a Nafion Membrane and an Advanced Sulfur Electrode

Xingwen Yu, Jorphin Joseph and Arumugam Manthiram*

A non-porous, cation-selective, lithiated Nafion membrane effectively suppresses the polysulfide-shuttle. The Li-S battery system with the lithiated Nafion membrane exhibits significantly enhanced cyclability compared to the cells with the traditional liquid-electrolyte integrated porous separator.